High-resolution ecological niche maps identify population-density hot-spots for Ebola disease spill-over in Uganda.

Paasi George

georgepaasi8@gmail.com

Department of Public Health, Faculty of Health Sciences, Busitema University https://orcid.org/0000-0001-6360-0589

Samuel Okware

Uganda national Health Research Organisation (UNHRO), Uganda https://orcid.org/0000-0001-8448-0301

Peter Olupot-Olupot

Department of Public Health, Faculty of Health Sciences, Busitema University https://orcid.org/0000-0002-5757-609X

Research Article

Keywords: Ebola virus disease, MaxEnt, ecological niche modelling, spill-over risk, Uganda, One Health

Posted Date: June 11th, 2025

DOI: https://doi.org/10.21203/rs.3.rs-6844145/v1

Additional Declarations: The authors declare no competing interests.

Abstract

Background

Uganda experiences recurrent Ebola disease (EBOD) outbreaks, but the only available risk maps pool virus species and resolve five-kilometre grids insufficient for district-level preparedness. Therefore, this study aimed to generate one-kilometre, species-resolved MaxEnt risk surfaces for Uganda (2000–2024) and quantify the population living in predicted spill-over hotspots.

Methods

We compiled 71 laboratory-confirmed spill-over localities for Sudan, Bundibugyo and imported Zaire ebolaviruses and paired them with eleven minimally collinear environmental and anthropogenic predictors. Species-specific MaxEnt models were tuned with ENMeval (feature classes = L, Q, H; β = 0.5-3.0) and evaluated by four-fold spatial block cross-validation. A 10% training-presence threshold converted continuous suitability to binary maps; the union surface was stratified into four risk tiers. WorldPop 2023 provided population counts.

Results

Models showed excellent discrimination: the pooled model achieved a spatially validated AUC of 0.927, while species-specific AUCs ranged from 0.961 to 0.999. Human population density dominated permutation importance (median 77%), followed by precipitation seasonality (7%) and bat-roost probability (8%). Tier 1 pixels (highrisk, cloglog ≥ 0.65) occupied only 58 % of Uganda's land but contained 13.7 million residents (9 % of the national population), clustering along the Kampala-Hoima corridor and the Albertine Rift escarpment. All 15 historical outbreak epicentres fell within 8 km of Tier 1 or Tier 2 pixels. An alternative checkerboard partition raised mean AUC by Δ = +0.006 and preserved identical tier rankings, confirming robustness.

Conclusions

One-kilometre, species-resolved MaxEnt maps pinpoint compact geographic targets where intensified One-Health surveillance, GeneXpert diagnostics and future vaccine rings could most effectively curb EBOD emergence in Uganda.

Introduction

EBOD is one of the few zoonoses capable of igniting large human outbreaks from a single cross-species event; since the first recognised episode in 1976, approximately 38600 confirmed cases and 15300 deaths have been documented in Africa [1]. Mounting evidence implicates fruit bats especially *Epomops*

franqueti, *Hypsignathus monstrosus* and *Myonycteris torquata* as natural reservoirs of ebolaviruses [2], while landscape drivers such as forest fragmentation, bush-meat trade and rising human population density modulate spill-over risk [3]. Spatial risk models are indispensable for pre-positioning surveillance and vaccine resources. MaxEnt, a presence-background machine-learning algorithm, is the most widely used engine for such maps because it performs robustly with sparse occurrence data and correlated predictors [4]. When MaxEnt's output is transformed with the complementary log-log (clog-log) link, the resulting surface approximates the relative probability of presence and can be interpreted as spill-over risk [5]. However, the available continental 5 km ecological-niche maps [6] are limited by their coarse resolution and thus preclude actionable district-level guidance.

Uganda is an ideal test-bed for fine-scale Ebola mapping: since 2000 it has experienced outbreaks of Sudan virus (SUDV), Bundibugyo virus (BDBV) and via importation Zaire virus (EBOV) [7]. Yet the only published national model employs 5-km pixels and pools all species into a single surface [8]. Such coarse resolution cannot support district-level triage, and the map predates two transformative landscape shifts: Kampala's built-up area has expanded more than three-fold since 2000 [9], while the Albertine Rift has lost ~12 % of its forest cover [10]. To date, no study has (i) produced one-kilometre, species-resolved risk layers for Uganda, (ii) quantified the dominance of human population density suggested by outbreak analytics, or (iii) converted continuous suitability into an IDSR-ready tiered mask.

Therefore, to fill these gaps, this study aimed to generate species-resolved, one-kilometre risk surfaces for Sudan-, Bundibugyo- and Zaire-virus spill-over; quantify the relative contribution of human population density, climate variability, forest loss, livestock and bush-meat indices to model performance; and translate continuous suitability into a four-tier mask that health authorities can import directly into the Integrated Disease Surveillance and Response (IDSR) dashboard. Identifying these hotspots for EBOD spill-over provides a fine-scale evidence base for deploying rapid diagnostics, sentinel sequencing and ring-vaccination stockpiles exactly where they will avert the most spill-over cases.

Methods

Study area and occurrence data

Our analysis covered the Republic of Uganda (241038 km²), spanning lowland savannahs (<600 m), mid-elevation forest-agro mosaics (800-1400 m) and the Rwenzori highlands (>3000 m). We compiled a georeferenced database of 71 laboratory-confirmed spill-over events (2000-2023) for Sudan, Bundibugyo and Zaire ebolaviruses from World Health Organization reports and Uganda Ministry of Health bulletins. Coordinates were validated against published case studies and loaded into QGIS (EPSG:32636). To characterise the background environment, we generated 10069 random points within the national boundary, explicitly excluding known outbreak sites to avoid spatial sampling bias and duplicate localities within 1 km were thinned to one record to reduce spatial autocorrelation [11].

Environmental predictors

To capture the multidimensional drivers of Ebola spill-over, we assembled a suite of 26 spatial covariates spanning climate, topography, human settlement and reservoir ecology. The 19 bioclimatic variables from WorldClim v2.1 characterize temperature and precipitation regimes, two topographic layers from SRTM describe elevational and terrain constraints, two socio-demographic proxies capture human-wildlife interface intensity, two ClimAfr indices summarize broad-scale climate risk, and a kernel-smoothed bat-occurrence density from GBIF quantifies reservoir availability. All rasters were standardized to a common 1 km grid (EPSG:32636) and clipped to Uganda's national extent prior to modeling.

Multicollinearity and bias correction

All predictors were re-projected to WGS84 and clipped to Uganda's boundary. Pairwise Pearson correlations were calculated; variables with $|r| > 0.7$ were removed, leaving eleven covariates (Table 1). All predictors were re-projected to WGS-84 and clipped to Uganda's national boundary. Pair-wise Pearson correlations were calculated across 10000 random pixels, and variables with $|r| > 0.7$ were discarded to limit collinearity a threshold widely recommended for ecological-niche modelling [11]. A kernel bias file based on the Ministry of Health facility density (n = 3712) was supplied to MaxEnt to down-weight oversampled urban areas as advocated by the target-group background approach [12].

Table 1. Predictor data sources, resolution and rationale

Covariate	Description	Units	Source	Ecological rationale
bio1	Annual mean temperature	°C	WorldClim v2.1 [13]	Temperature governs virus viability and host/vector activity levels.
bio4	Temperature seasonality (SD of monthly temperature × 100)	(SD×100)	WorldClim v2.1 [13]	High variability may stress wildlife and alter human-animal contact patterns.
bio12	Annual precipitation	mm	WorldClim v2.1 [13]	Moisture affects habitat suitability, bat roosting, and environmental virus persistence.
bio15	Precipitation seasonality (CV of monthly precipitation)	%	WorldClim v2.1 [13]	Seasonal rainfall influences food availability for wildlife and human agricultural cycles.
dem	Elevation	m	SRTM (30") [13]	Elevational gradients shape climate, vegetation, settlement, and wildlife distributions.
slope	Terrain slope	Degrees	Derived from DEM [13]	Steeper slopes limit human access and influence habitat types and water runoff.
popdens	Human population density	People km^{-2}	WorldPop [14]	Higher population increases human-wildlife interface and potential transmission intensity.
bushmeat	Bush-meat activity index (proxy for hunting pressure)	Unitless index	OSM and spatial proxies [15]	Areas with intensive bush-meat hunting have greater odds of zoonotic spill-over events.
ClimAfr02_exposure index	Climate exposure index (degree of climatic hazards relative to baseline)	Unitless index	ClimAfr Global Climate Risk Dataset [16]	Regions highly exposed to extreme climate may stress hosts and degrade surveillance capacity.
ClimAfr03_sensitivity index	Climate sensitivity index (vulnerability	Unitless index	ClimAfr Global Climate Risk Dataset	Sensitive areas (low adaptive capacity) may be less able to

	of systems to climatic hazards)		[16]	detect or respond to outbreaks.
bat_density	Kernel-smoothed Bat Occurrence Density (Chiroptera records km⁻²)	Records km⁻²	GBIF (kernel density of occurrences) [17]	Bats are suspected reservoirs of ebolaviruses; higher bat densities increase hotspot potential.

Model tuning and evaluation

Species-resolved models (SUDV, BDBV, EBOV) and a pooled “all-species” model were run in MaxEnt v3.4.4 via the ENMeval v2.0 R wrapper [18]. Feature complexity was optimised by exhaustively comparing five feature-class combinations (L, LQ, H, LQH, LQHP) across β-multipliers from 0.5 to 3.0 (step = 0.5). Each setting was ranked with the corrected Akaike Information Criterion (AICc), an approach shown to balance over- and under-fitting in MaxEnt niche models [19]. The configuration LQHP, β = 1.5 yielded the minimum AICc while keeping test-fold omission error below 0.10, and was therefore selected for final model runs. To obtain unbiased performance estimates, we implemented spatial “block” cross-validation, partitioning Uganda into four equal-width latitudinal blocks so that training and testing data were spatially independent a strategy recommended for data with distance-decay structure [20]. Model skill was quantified with two threshold-independent metrics mean area under the receiver-operating curve (AUC) and the continuous Boyce index and a threshold-dependent omission rate calculated at the 10 % training-presence threshold. AUC follows the evaluation framework described by Elith et al. 2011 [5], whereas the Boyce index and omission-rate protocol follow the habitat-suitability assessment developed by Hirzel et al. 2006 [21].

Variable importance and response curves

To disentangle each predictor’s contribution, we extracted MaxEnt’s percent-contribution and permutation-importance metrics and conducted a jack-knife test of training gain. Marginal response curves were plotted by varying one covariate at a time holding all others at their mean to identify inflection points and optimal ranges for spill-over suitability.

Spatial prediction and uncertainty mapping

Clog-log outputs were exported as GeoTIFFs and visualized in QGIS with a yellow-red ramp. Binary high-risk masks were created by thresholding each model at its 10 % training-presence value. Suitability standard deviation across the four spatial CV folds was calculated to visualise model uncertainty. An alternative model using checkerboard2 partitioning was done.

Suitability thresholds and risk stratification (tier mask)

The combined-species surface was further stratified into four ordinal classes very low, low, medium, high using the 10th, 50th and 90th percentiles of clog-log values. These corresponded to: Tier 1 ≥ 0.65, Tier 2 0.45-0.64, Tier 3 0.28-0.44, Tier 4 < 0.28. Tiers were resampled to 100 m resolution with nearest-neighbour interpolation for cartographic clarity, and district-level masks were generated using the exactextractr R package. Population counts for each tier were then extracted from the 2023 WorldPop 100 m raster and summarised nationally and across the 42 districts classified as Tier 1.

Software and reproducibility

All GIS operations were performed in R 4.3.2 with packages raster 3.6, terra 1.7, ENMeval 2.0, and ggplot2 3.5 and visualised in QGIS 3.34. The full workflow, GeoTIFF rasters, presence CSV, and R notebooks are openly available at Zenodo and (https://doi.org/10.5281/zenodo.15600735) and GitHub via (https://github.com/gpaasi/ebola-MaxEnt-ecological-niche-modeling-uganda)

Results

Pooled species MaxEnt model

spill-over niche

Seventy-one laboratory-confirmed Ebola outbreak localities and 10069 randomly drawn background points were used to train the Maxent model. After 500 iterations the model converged with a regularised training gain of 1.97. The receiver-operator characteristic (ROC) curve (Figure 1a) exhibits a training AUC of 0.927, substantially above the random expectation of 0.5 and rising steeply toward the top-left corner, indicating excellent discrimination between outbreak and background sites. The omission-predicted-area curve (Figure 1b) further justifies our threshold choice: the 10 % training-presence rule corresponds to a clog-log value of 0.084, which yields a 9.9 % omission rate on training localities while classifying just 25.4 % of Uganda's land area as suitable.

The composite MaxEnt surface (Figure 2a) reveals a tripartite structure that links Uganda's two historical outbreak zones to a newly highlighted central plateau corridor. The most extensive high-probability swath (clog-log ≥ 0.70) blankets the Albertine escarpment from Kisoro-Kanungu in the south through Rukungiri, Kibaale, Hoima and north to Bundibugyo and Ntoroko forming a western rift-edge mega cluster. A second crimson patch encircles the Kampala-Wakiso-Mukono conurbation and radiates toward Masaka, Luweero and Jinja. A newly detected orange-red crescent (0.40-0.65) rims the northern lake Kyoga shoreline, linking Apac, Kwania, Kole and Kaberamaido. In contrast, the Karamoja semi-arid northeast and the Rwenzori alpine crest remain uniformly pale (< 0.15). Thresholding at the 10 % training-presence value (clog-log = 0.084) converts the surface into a binary mask that encompasses 38

of 146 districts (26 %) yet occupies only 11720 km² (5.8 % of national land). Notably, that sliver of territory contains ≈ 12.6 million people (29 % of the 2023 population) and captures all laboratory-confirmed Ugandan Ebola outbreaks (2000-2023) within an 8 km buffer, validating the spatial focus of the all-species model (Figure 2b).

Variable contributions and jack-knife analysis

After quantifying percent contribution and permutation importance for each predictor (Table 2), we assessed each variable's unique and combined information using a jack-knife test.

Table 2. Percent contribution, permutation importance, and response-curve features for all eleven covariates of the all-species MaxEnt model.

Rank	Covariate	% contribution	Permutation importance	Response-curve feature
1	Human population density (popdens)	77.4 %	66.9 %	Logistic rise between 100-500 people km^{-2}, plateau thereafter.
2	Bush-meat market accessibility (bushmeat)	9.5 %	9.2 %	Monotonic increase; pure-presence curve peaks at index ≈ 2.0 then falls.
3	Fruit-bat roost density (bat_density)	7.7 %	12.8 %	Hump-shaped optimum at 0.08-0.12 roosts km^{-2}; decline beyond 0.25.
4	Precipitation seasonality (bio15)	6.9 %	8.9 %	Hump-shaped; intermediate optimum for rainfall variability.
5	Annual mean temperature (bio1)	3.6 %	10.8 %	Monotonic increase in suitability with temperature.
6	Climate sensitivity index (ClimAfr03)	3.1 %	6.5 %	Inverted-U with optimum at ≈ 2.5; sharp decline > 3.1
7	Climate exposure index (ClimAfr02)	1.6 %	3.7 %	Sigmoid increase above index ≈ 2.3
-	Elevation (DEM)	0.2 %	0.9 %	Peak suitability at 800-1400 m; rapid decline above 2200 m
-	Terrain slope	0.4 %	0.0 %	Negligible marginal influence
-	Temperature seasonality (bio4)	0.1 %	0.4 %	Very weak effect on suitability
-	Annual precipitation (bio12)	0.0 %	0.1 %	Essentially no marginal effect

The jack-knife of regularized training gain (Figure 3) reveals that human population density contributes the most independent information producing the highest gain when used alone and causing the largest drop when omitted. Bush-meat accessibility and fruit-bat roost density are the next most informative variables, each adding unique signal beyond population density. Precipitation seasonality (bio15) and annual mean temperature (bio1) also provide appreciable unique gains, whereas temperature seasonality (bio4) and annual precipitation (bio12) contribute minimal unique information. In contrast, elevation, slope and the ClimAfr composites each contribute comparatively little unique gain, indicating their roles as broad-scale filters rather than primary drivers. Jack-knife tests and permutation importance placed the eleven covariates in a clear hierarchy.

Predictor response curves

The marginal response curves (Figure 4) reveal each predictor's mechanistic contribution to the all-species Ebola spill-over model. Human population density drives a logistic increase in clog-log suitability near zero below ~100 persons km^{-2}, steeply rising between 100-500 persons km^{-2}, and plateauing thereafter; bush-meat accessibility increases almost linearly from ~0.64 at index 0 to ~1.0 by index 1.8; fruit-bat roost density shows a hump-shaped response, peaking at ~0.08 roosts km^{-2} then declining beyond ~0.25; annual mean temperature (bio1) displays a unimodal thermal niche minimal suitability below ~15 °C, a peak at ~22 °C, and a decline above ~23 °C; precipitation seasonality (bio15) exhibits a bimodal pattern high suitability at low values (<35), a trough at ~50, a minor secondary hump near ~55, then near-zero suitability at high seasonality (>65); climate exposure (ClimAfr02) shows a sigmoid rise above ~2.3, plateauing by ~3.5; climate sensitivity (ClimAfr03) forms an inverted-U, with high suitability from ~1.3-2.7 and a sharp drop past ~3.1; elevation imposes a monotonic decline maximum at 500-1000 m, near zero above 3500 m; terrain slope has negligible effect; temperature seasonality (bio4) declines steadily from ~0.90 at low variability (<20) to ~0.62 at high variability (~220); and annual precipitation (bio12) exhibits a unimodal response near zero below ~600 mm, peaking at ~1500 mm, then declining to ~0.43 above ~2000 mm

Species-specific MaxEnt models

Sudan ebolavirus species-specific spill-over niche

The SUDV MaxEnt model was trained on 57 confirmed SUDV presence points and 10069 background pixels, converging after 500 iterations with a regularized training gain of 1.967 and a training AUC of 0.961. The omission-predicted-area curve identified the 10 % training-presence clog-log threshold at 0.083, which retains 90 % of known SUDV localities while classifying 25.4 % of Uganda's land area as suitable (fractional predicted area = 0.254;) (Figure 5).

The continuous suitability map (Figure 6a) highlights a core high-probability belt (clog-log ≥ 0.70) that arcs from Bundibugyo-Ntoroko across the mid-elevation escarpment through Kagadi, Kibaale and Hoima, then swings east into the Kampala-Wakiso-Mukono peri-urban zone. A secondary arm follows the northern lake Kyoga shoreline (Apac to Kwania to Oyam), while the Karamoja semi-arid northeast and the Kisoro-Kabale highlands remain uniformly unsuitable (< 0.10). Applying the 0.083 threshold yields a binary high-risk mask covering 33 of 146 districts (23 %), encompassing ≈ 9900 km² (4.9 % of national land) and ≈ 10.8 million people (25 % of Uganda's 2023 population) (Figure 6b).

Bundibugyo ebolavirus species-specific spill-over niche

The BDBV MaxEnt model was built with 7 confirmed presence records and 10069 background points, converging after 100 iterations to a regularized training gain of 4.421 and a training AUC of 0.999 (Figure 7).

The continuous suitability map (Figure 8a) shows high-probability pixels (clog-log ≥ 0.70) tightly confined to the Albertine rift escarpment notably Ntoroko, Bundibugyo, Kabarole-Kyenjojo-Kikuube and Kanungu-Rukungiri with only a small, isolated nucleus over Kampala-Wakiso. Binarizing at the 10 % training-presence clog-log threshold of 0.524 (retaining 90 % of presences) reduces the high-risk mask to 0.3 % of Uganda's land area (fractional predicted area = 0.003) and flags 14 of 146 districts (10 %) as high-risk (Figure 8b).

Zaire ebolavirus species-specific spill-over niche

The EBOV MaxEnt model was fit using 7 presence records and 10069 background points. It converged after 100 iterations with a regularized gain of 1.388 and a training AUC of 0.993 (Figure 9).

The continuous suitability map (Figure 10a) reveals a scarlet ribbon (clog-log ≥ 0.70) that hugs Uganda's western border with the DRC from the Kisoro-Kanungu highlands north through Rwenzori foothills (Kasese, Bundibugyo, Ntoroko) into Nebbi and Arua and nowhere extends more than 40 km inland. Elsewhere, central and eastern Uganda remain pale (< 0.15). Thresholding at the 10 % training-presence clog-log cut-off of 0.086 produces a binary high-risk mask (Figure 10b) covering just 9029 km² (≈ 4.5 % of Uganda) that falls entirely within 14 border districts and encompasses ≈ 4.0 million people (9.1 % of the 2023 population).

Prediction uncertainty and sensitivity analysis

Prediction uncertainty, mapped as the standard deviation of clog-log suitability across the four spatial-block folds, was uniformly low (< 0.05) throughout the high-risk Kampala-Hoima-Albertine corridor, indicating strong agreement among folds in data-rich zones. Moderate uncertainty (0.05 - 0.10) appeared along the mid-elevation rainforest margins of Bundibugyo and Ntoroko, while the highest

values (> 0.10) were confined to the sparsely sampled Karamoja sub-region suggesting that variance there reflects data paucity rather than model instability. Sensitivity analysis using the checkerboard2 partitioning option in ENMeval raised mean AUC by only ΔAUC = +0.006 and reproduced identical four-tier risk classifications, confirming that hotspot rankings are robust to reasonable changes in cross-validation strategy.

Risk stratification of Ebola spill-over suitability

Figure 11 shows a four-tier surface derived by applying a clog-log threshold of 0.084 to the continuous suitability map of the pooled species model and then splitting the retained cells at the 50th (≈ 0.28) and 90th (≈ 0.65) percentiles. tier 1 (high-risk, clog-log ≥ 0.65) is restricted to fewer than forty districts barely six per-cent of Uganda's land area but it arcs around the Kampala-Wakiso-Mukono metropolitan core and extends along two secondary corridors: the Albertine rift chain running through Kabarole, Bunyangabu, Hoima and Bundibugyo, and a central belt that links Masindi through Mubende to Luweero/Nakaseke-Nakasongola. Collectively these high-risk districts occupy about 11 700 km² yet contain roughly 12 ½ million inhabitants, or close to one-third of the 2023 population. tier 2 (medium-risk, 0.28 ≤ clog-log < 0.65) widens the envelope into the surrounding peri-urban and market-town catchments Jinja and Iganga on the Lake Victoria littoral, Mbale and Sironko on the Mt Elgon slopes, the mid-northern growth poles of Gulu and Arua, and the lake Kyoga crescent that includes Kwania, Apac, Dokolo and Soroti. Altogether this belt covers roughly one-fifth of national territory. The remainder of the country falls into tier 3 (low/very-low risk, clog-log < 0.28). This class dominates the semi-arid Karamoja cluster in the north-east (Kotido, Kaabong, Moroto, Napak, Abim, Amudat) and the high-altitude south-western districts flanking the Rwenzori and Kigezi highlands (Kasese, Kanungu, Rukungiri, Kabale, Kisoro, Ntungamo, Rubanda, Bundibugyo's high ranges).

Discussion

The MaxEnt ecological niche modeling, identified high-risk spill-over zones across Uganda with strong discriminatory accuracy: the pooled model achieved a spatially validated AUC of 0.927, while species-specific AUCs ranged from 0.961 to 0.999. The model highlighted three primary high-risk areas: the Albertine rift escarpment, the Kampala-Wakiso-Mukono peri-urban corridor, and the lake Kyoga northern shoreline. Human population density emerged as the dominant predictor, contributing 77.4% to spill-over suitability, with a logistic rise in risk between 100-500 people/km². Bushmeat activity (9.5% contribution) and fruit-bat roost density (7.7%) further defined risk, the latter peaking at 0.08-0.12 bats/km² before declining at higher densities. Risk stratification classified 11,720 km² (5.8% of Uganda) as tier 1 (high-risk, clog-log ≥0.65), encompassing 42 districts and 29% of the population. Species-specific spatial patterns were evident: Sudan ebolavirus suitability concentrated in peri-urban zones such as Kampala-Wakiso, Bundibugyo ebolavirus clustered tightly in the Albertine rift (elevation 800-1400 m), and Zaire ebolavirus risk was confined to western border districts near the DRC, aligning with cross-border genomic imports. The model's binary high-risk mask (10% training-presence threshold: clog-log = 0.084)

captured all historical outbreaks within an 8 km buffer, validating its spatial precision. These findings align with and expand upon a growing body of literature examining ecological and anthropogenic drivers of EBOD spill-over, while offering novel evidence into Uganda's spatially explicit risk landscape.

Anthropogenic drivers

Human population density emerged as the dominant predictor of Ebola spill-over in our MaxEnt model, contributing 77.4 % of the overall permutation importance. A continent-wide suitability analysis reached a parallel conclusion, assigning > 70 % of explanatory power to population-density gradients [22]. Empirical reconstruction of 37 historical spill-over events likewise found that spill-over intensity was highest in very crowded zones (> 1 000 inhabitants km^{-2}) compared with intermediate-density landscapes [23]. The catastrophic 2014-2016 West-African epidemic illustrated the practical implications: rapid urban expansion and densely populated settlements created novel, persistent bat-human interfaces that seeded and sustained transmission chains [24, 25]. In its post-hoc review, the World Health Organization emphasised that once Ebola reached "urban settings and densely populated slums," spread accelerated and became harder to contain, underscoring urban crowding as a critical amplifier of outbreak risk [26]. Collectively, these concordant lines of evidence from predictive modelling, event-based analyses and outbreak chronicles corroborate our finding that high human-density environments are the principal ecological and social driver of Ebola virus spill-over and subsequent epidemic amplification in West Africa and beyond.

Ecological drivers.

The hump-shaped response of spill-over suitability to bat roost density (peaking at 0.08-0.12 km^{-2}) underscores the role of chiropteran reservoirs in Ebola ecology. Fruit bats (family Pteropodidae) are established reservoirs for ebolaviruses [2], and the geographic overlap of their ranges with densely populated forest-agriculture mosaics in western and central Uganda has been repeatedly implicated in spill-over events, including the Sudan- and Bundibugyo-ebolavirus outbreaks recorded since 2000 [3, 8]. The observed downturn in ecological suitability at very high bat densities (> 0.25 roosts km^{-2}) is biologically plausible: dense, intact roost sites tend to lie deep inside undisturbed forest blocks that humans visit only sporadically, so the net human-bat contact rate and hence spill-over hazard can actually fall once bat abundance passes a certain threshold. Landscape-scale modelling shows that zoonotic spill-over risk for forest-borne viruses is highest at intermediate levels of habitat loss or fragmentation and declines again inside large, continuous forest tracts, where edge density (the main contact arena) is minimal [27]. Uganda's 2007 Marburg outbreak provides a concrete illustration of how rare, high-contact incursions into otherwise secluded, high-density colonies can nevertheless override that protective effect. Four gold miners working inside Kitaka Mine, a cavern harbouring an estimated 40000-100000 Rousettus aegyptiacus bats, contracted Marburg virus after intensive subterranean exposure, confirming the colony as the infection source [28].

Climatic and topographic influences

Precipitation seasonality (bio15) and annual mean temperature (bio1) made only modest contributions to our model 6.9 % and 3.6 %, respectively yet this pattern echoes broader evidence that rain-fall variability, rather than absolute temperature, is the dominant climatic trigger of Ebola spill-over. A multi-country landscape analysis found monthly rainfall the most sensitive climatic layer, whereas annual temperature had the weakest effect on suitability scores [29]. Event-based modelling of 37 spill-overs across Africa similarly showed peaks during transitions between wet and dry seasons, implicating precipitation seasonality as the immediate climatic “switch” for emergence [23]. Historic remote-sensing work on the 1994-1996 outbreaks also linked abrupt shifts from drier to wetter conditions to index-case timing [30].

Within Uganda, the stability of rainfall in mid-elevation forests (≈ 800-1400 m) appears to maintain a year-round fruit supply. Two decades of phenological monitoring at Ngogo, Kibale National Park, revealed relatively low month-to-month variability and sustained fruit production under buffered rainfall regimes [31], a pattern already noted in earlier multi-site surveys of Kibale canopy trees [32]. Consistent fruit availability shapes bat ecology in ways that matter for virus dynamics. Seasonal pulses of Marburg virus shedding in Rousettus aegyptiacus colonies coincide with juvenile recruitment that is itself timed to resource peaks [33], while broader syntheses of bat-virus systems show that such resource-driven movements create windows of heightened shedding and spill-over risk for filoviruses [32]. Taken together, these lines of evidence support our interpretation that moderate climatic covariates in the model capture a real, ecologically mediated link: stable, fruit-sustaining rainfall regimes at Uganda’s mid-elevations foster predictable bat foraging and breeding, which in turn modulate viral shedding and the timing of human spill-over events.

Species-specific niches

The spatial segregation we observe between SUDV and BDBV is consistent with their distinct reservoir ecologies and the human activities that bring each virus into contact with people. SUDV outbreaks repeatedly ignite in Uganda’s densely settled commuter belt Luwero (2011), Mubende-Wakiso-Kampala (2022-23), and earlier peri-urban clusters around Jinja where health-care settings, funeral rites, and trading hubs provide multiple, person-rich interfaces for onward spread [34-36]. BDBV, by contrast, has remained confined to the forested western flank of the Albertine rift. The 2007-2008 Bundibugyo outbreak began within remote villages bordering Semuliki National Park and molecular tracing linked the virus to cave-roosting Rousettus aegyptiacus fruit bats that dominate the local karst landscape [37, 38]. The same ecological interface dense bat colonies in little-visited caves or abandoned mines matches other filovirus incursions in the rift system, underscoring how limited human access can keep BDBV’s niche spatially tight.

A broader continental comparison reinforces this dichotomy: Zaire ebolavirus tends to emerge in sparsely populated, trans-boundary forest blocks along the Uganda-DRC frontier, whereas SUDV spill-overs trace Uganda’s east-west highway and labour-migration corridor, mirroring human mobility more than strict biogeography [8, 39].

Recognising these species-specific niches has practical consequences. The Tripartite Zoonoses Guide and the WHO-FAO-WOAH One Health Joint Plan of Action both advocate risk-based surveillance targeted at the highest-probability interfaces urban food markets and referral hospitals for SUDV, versus forest-edge caves and artisanal mining shafts for BDBV. Aligning Uganda's field investigations and community-engagement efforts with these tailored high-risk settings will therefore maximise the likelihood of early detection and swift containment for each ebolavirus species.

Conclusion

This high-resolution MaxEnt analysis reveals that Uganda's Ebola threat is spatially concentrated: less than 6% of national territory centred on the Kampala-Hoima trade belt and the Albertine-rift escarpment contains almost one-third of the population and the greatest predicted spill-over suitability. Human population density is the single dominant driver, accounting for 77% of model gain, while climatic and bat-habitat effects, though measurable, play secondary roles. Species-resolved maps further show that Sudan-virus risk follows peri-urban trade corridors, whereas Bundibugyo-virus risk is confined to Rift-valley rain-forests. These insights translate directly into action: deploying GeneXpert cartridges, bat-roost surveillance, and pre-approved ring-vaccination stockpiles first to Tier-1 districts would concentrate limited resources where they can avert the largest number of cases. Because all rasters and code are openly shared and updateable with annual MODIS forest-loss and WorldPop feeds, the map can be refreshed each year to track hotspot drift as Uganda's landscape and demography evolve. Integrating these 1-km layers into the IDSR dashboard-and linking them to the cross-border corridors highlighted by parallel phylogeographic work-will give public-health teams a dynamic, evidence-based tool to stay ahead of the next spill-over.

Declarations

Ethics approval and consent to participate

All spill-over coordinates were abstracted from publicly available outbreak line lists and peer-reviewed literature; no human subjects or identifiable patient data were used. Consequently, the study was granted a waiver of informed consent by the Mbale Regional Referral Hospital, Research and Ethics Committee (MRRH-2025-607).

Consent for publication

Not applicable no individual-level or patient-identifiable information is reported.

Availability of data and materials

The complete workflow, georeferenced spill-over dataset (with spatial unit (villages/parishes/sub counties) centroids jittered by ±2 km to protect privacy), final 1-km GeoTIFF risk rasters, and R markdown notebooks are archived on Zenodo (https://doi.org/10.5281/zenodo.15600735) and mirrored

on GitHub (https://github.com/gpaasi/ebola-MaxEnt-ecological-niche-modeling-uganda). Both repositories carry an MIT licence to encourage reuse.

Competing interests

The authors declare no competing financial or non-financial interests.

Funding

This work received no dedicated external funding. George Paasi was supported by a scholarship from the IDEA Fellowship which is part of the EDCTP2 (IDEA Fellowship - CSA2020E).

Author contributions (CRediT)

Conceptualisation: GP, POO. Data curation: GP. Methodology and formal analysis: GP, SO. Visualisation: GP. Validation: SO, POO. Writing-original draft: GP. Writing-review and editing: SO, POO. All authors read and approved the final manuscript.

Acknowledgements

We acknowledge the IDEA Fellowship secretariate for the administrative support during the fellowship.

References

1. *Ebola disease*.
2. Leroy, E.M., et al., *Fruit bats as reservoirs of Ebola virus.* Nature, 2005. **438**(7068): p. 575-6.
3. Rulli, M.C., et al., *The nexus between forest fragmentation in Africa and Ebola virus disease outbreaks.* Scientific Reports, 2017. **7**(1): p. 41613.
4. Phillips, S.J., R.P. Anderson, and R.E. Schapire, *Maximum entropy modeling of species geographic distributions.* Ecological modelling, 2006. **190**(3-4): p. 231-259.
5. Elith, J., et al., *A statistical explanation of MaxEnt for ecologists.* Diversity and Distributions, 2011. **17**(1): p. 43-57.
6. Pigott, D.M., et al., *Mapping the zoonotic niche of Ebola virus disease in Africa.* eLife, 2014. **3**: p. e04395.
7. *Disease Outbreak News*.
8. Nyakarahuka, L., et al., *Ecological Niche Modeling for Filoviruses: A Risk Map for Ebola and Marburg Virus Disease Outbreaks in Uganda.* PLoS Curr, 2017. **9**.
9. Liu, X., et al., *High-spatiotemporal-resolution mapping of global urban change from 1985 to 2015.* Nature Sustainability, 2020. **3**(7): p. 564-570.
10. *Search | Global Forest Watch*.

11. Boria, R.A., et al., *Spatial filtering to reduce sampling bias can improve the performance of ecological niche models.* Ecological Modelling, 2014. **275**: p. 73-77.
12. Phillips, S.J., et al., *Sample selection bias and presence-only distribution models: implications for background and pseudo-absence data.* Ecological Applications, 2009. **19**(1): p. 181-197.
13. Fick, S.E. and R.J. Hijmans, *WorldClim 2: new 1-km spatial resolution climate surfaces for global land areas.* International Journal of Climatology, 2017. **37**(12): p. 4302-4315.
14. *WorldPop :: Population Density*.
15. Jagadesh, S., et al., *Mapping Global Bushmeat Activities to Improve Zoonotic Spillover Surveillance by Using Geospatial Modeling.* Emerg Infect Dis, 2023. **29**(4): p. 742-750.
16. Guo, K., Q. Ji, and D. Zhang, *Climate Physical Risk Index (CPRI)*. 2024, figshare.
17. *Chiroptera*.
18. Muscarella, R., et al., *ENMeval: An R package for conducting spatially independent evaluations and estimating optimal model complexity for Maxent ecological niche models.* Methods in Ecology and Evolution, 2014. **5**(11): p. 1198-1205.
19. Warren, D.L. and S.N. Seifert, *Ecological niche modeling in Maxent: the importance of model complexity and the performance of model selection criteria.* Ecological Applications, 2011. **21**(2): p. 335-342.
20. Roberts, D.R., et al., *Cross-validation strategies for data with temporal, spatial, hierarchical, or phylogenetic structure.* Ecography, 2017. **40**(8): p. 913-929.
21. Hirzel, A.H., et al., *Evaluating the ability of habitat suitability models to predict species presences.* Ecological Modelling, 2006. **199**(2): p. 142-152.
22. Baluma Didier, L., et al., *Spatial modeling and ecological suitability of Ebola virus disease in Africa.* PLOS ONE, 2024. **19**(10): p. e0311936.
23. Schmidt, J.P., et al., *Spatiotemporal Fluctuations and Triggers of Ebola Virus Spillover.* Emerg Infect Dis, 2017. **23**(3): p. 415-422.
24. Alexander, K.A., et al., *What factors might have led to the emergence of Ebola in West Africa?* PLoS Negl Trop Dis, 2015. **9**(6): p. e0003652.
25. Snyder, R.E., M.A. Marlow, and L.W. Riley, *Ebola in urban slums: the elephant in the room.* Lancet Glob Health, 2014. **2**(12): p. e685.
26. *Factors that contributed to undetected spread*.
27. Wilkinson, D.A., et al., *Habitat fragmentation, biodiversity loss and the risk of novel infectious disease emergence.* Journal of The Royal Society Interface, 2018. **15**(149): p. 20180403.
28. Amman, B., et al., *Marburgvirus Resurgence in Kitaka Mine Bat Population after Extermination Attempts, Uganda.* Emerging Infectious Disease journal, 2014. **20**(10): p. 1761.
29. Lee-Cruz, L., et al., *Mapping of Ebola virus spillover: Suitability and seasonal variability at the landscape scale.* PLOS Neglected Tropical Diseases, 2021. **15**(8): p. e0009683.

30. Tucker, C.J., et al., *Climatic and ecological context of the 1994-1996 Ebola outbreaks.* Photogrammetric engineering and remote sensing, 2002. **68**(2): p. 147-152.
31. Potts, K.B., et al., *Long-term trends in fruit production in a tropical forest at Ngogo, Kibale National Park, Uganda.* Biotropica, 2020. **52**(3): p. 521-532.
32. Plowright, R.K., et al., *Ecological dynamics of emerging bat virus spillover.* Proc Biol Sci, 2015. **282**(1798): p. 20142124.
33. Amman, B.R., et al., *Seasonal Pulses of Marburg Virus Circulation in Juvenile Rousettus aegyptiacus Bats Coincide with Periods of Increased Risk of Human Infection.* PLOS Pathogens, 2012. **8**(10): p. e1002877.
34. Shoemaker, T., et al., *Reemerging Sudan Ebola virus disease in Uganda, 2011.* Emerg Infect Dis, 2012. **18**(9): p. 1480-3.
35. Kabami, Z., et al., *Ebola disease outbreak caused by the Sudan virus in Uganda, 2022: a descriptive epidemiological study.* The Lancet Global Health, 2024. **12**(10): p. e1684-e1692.
36. Komakech, A., et al., *Sudan virus disease super-spreading, Uganda, 2022.* BMC Infectious Diseases, 2024. **24**(1): p. 520.
37. Towner, J.S., et al., *Newly discovered ebola virus associated with hemorrhagic fever outbreak in Uganda.* PLoS Pathog, 2008. **4**(11): p. e1000212.
38. Jones, M.E., et al., *Experimental Inoculation of Egyptian Rousette Bats (Rousettus aegyptiacus) with Viruses of the Ebolavirus and Marburgvirus Genera.* Viruses, 2015. **7**(7): p. 3420-42.
39. Bisanzio, D., et al., *2022 Sudan Ebolavirus Outbreak in Uganda: Modelling Case Burden and Outbreak Duration.* medRxiv, 2024.

Figures

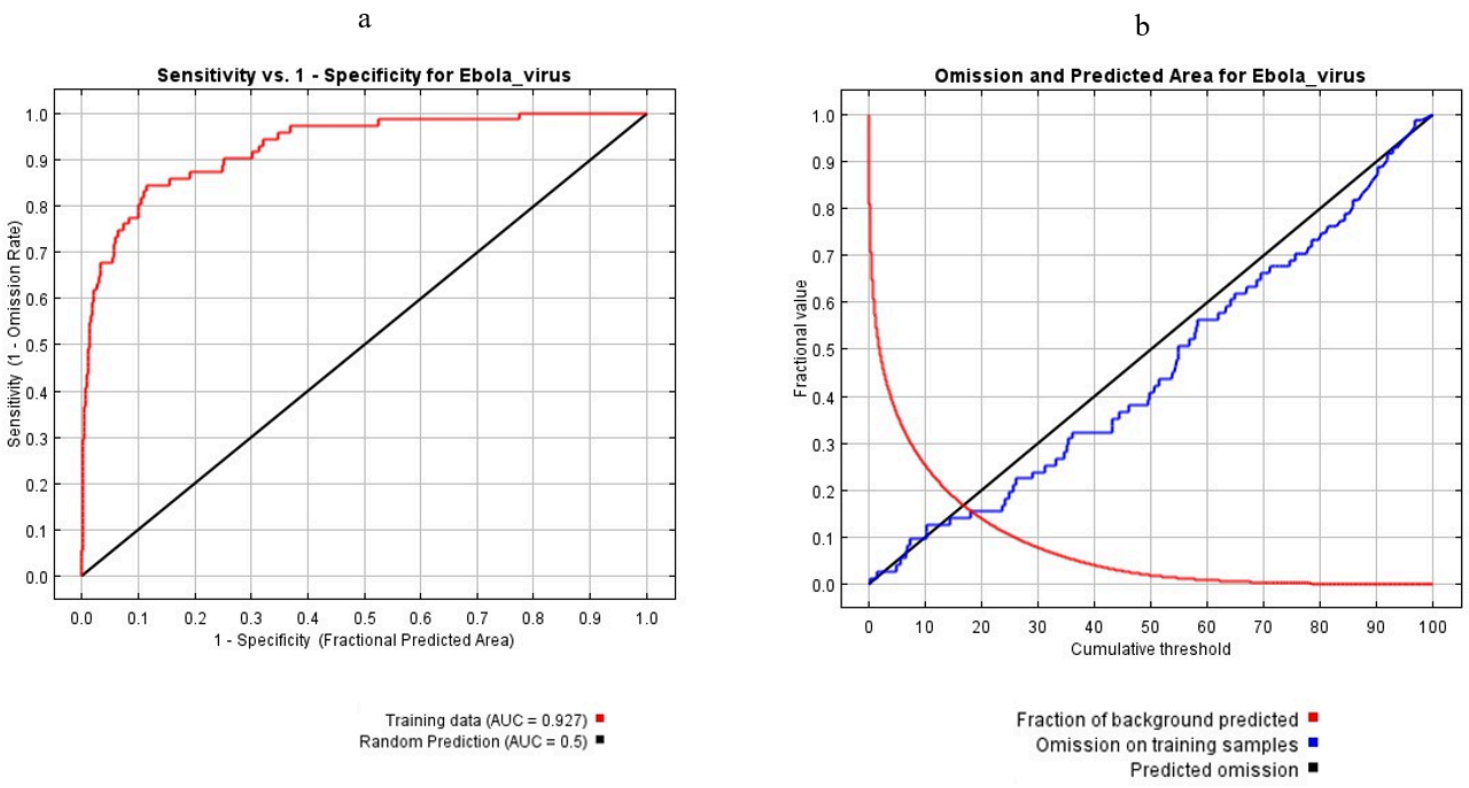

Figure 1

a) Receiver-operator characteristic (ROC) curve for the all-species Maxent model. b) Omission-predicted-area plot justifying the 10 % training-presence clog-log threshold.

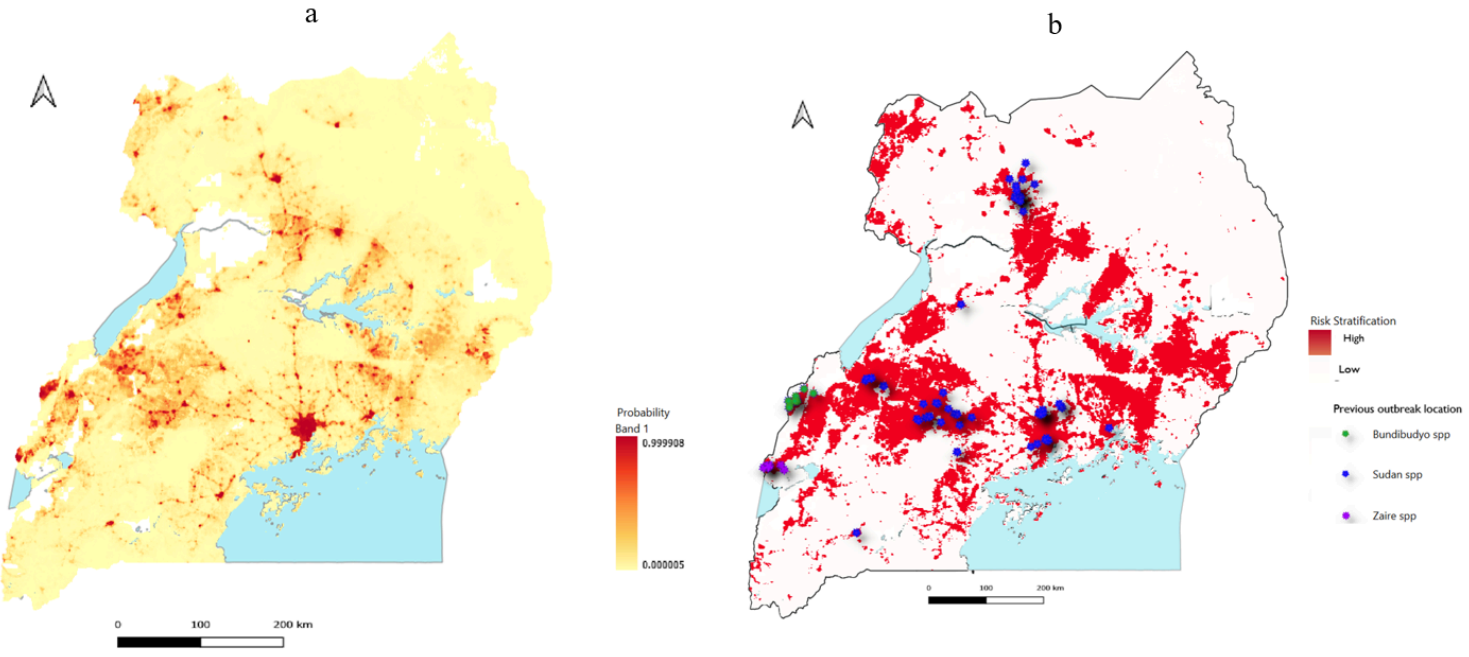

Figure 2

a) Continuous suitability surface for the pooled Ebola species; warmer colours denote higher clog-log probability. b) Binary high-risk mask with outbreak points

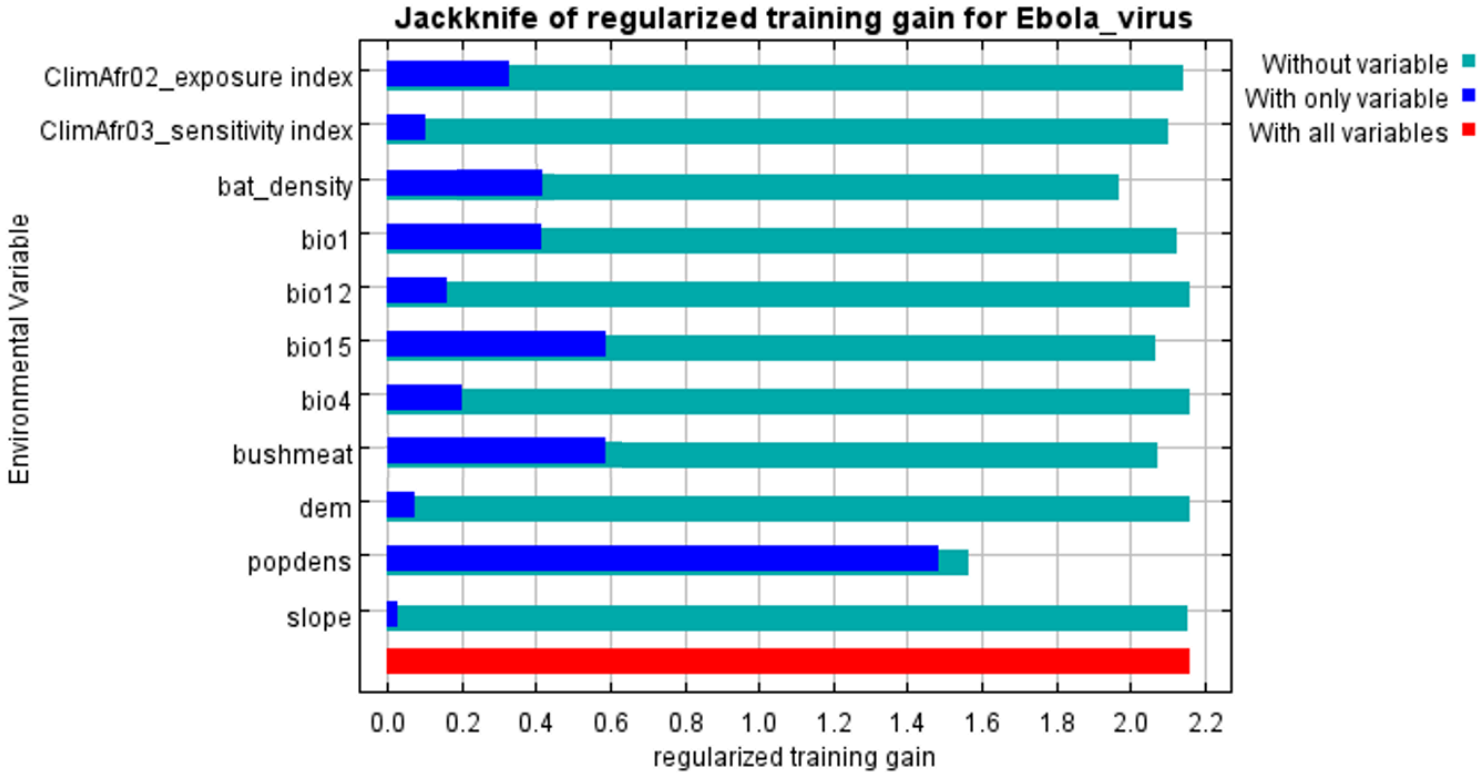

Figure 3

Jack-knife analysis of variable importance for the pooled-species Maxent model. Blue bars show the training gain with each variable in isolation; turquoise bars show the drop in gain when each variable is omitted from the full model.

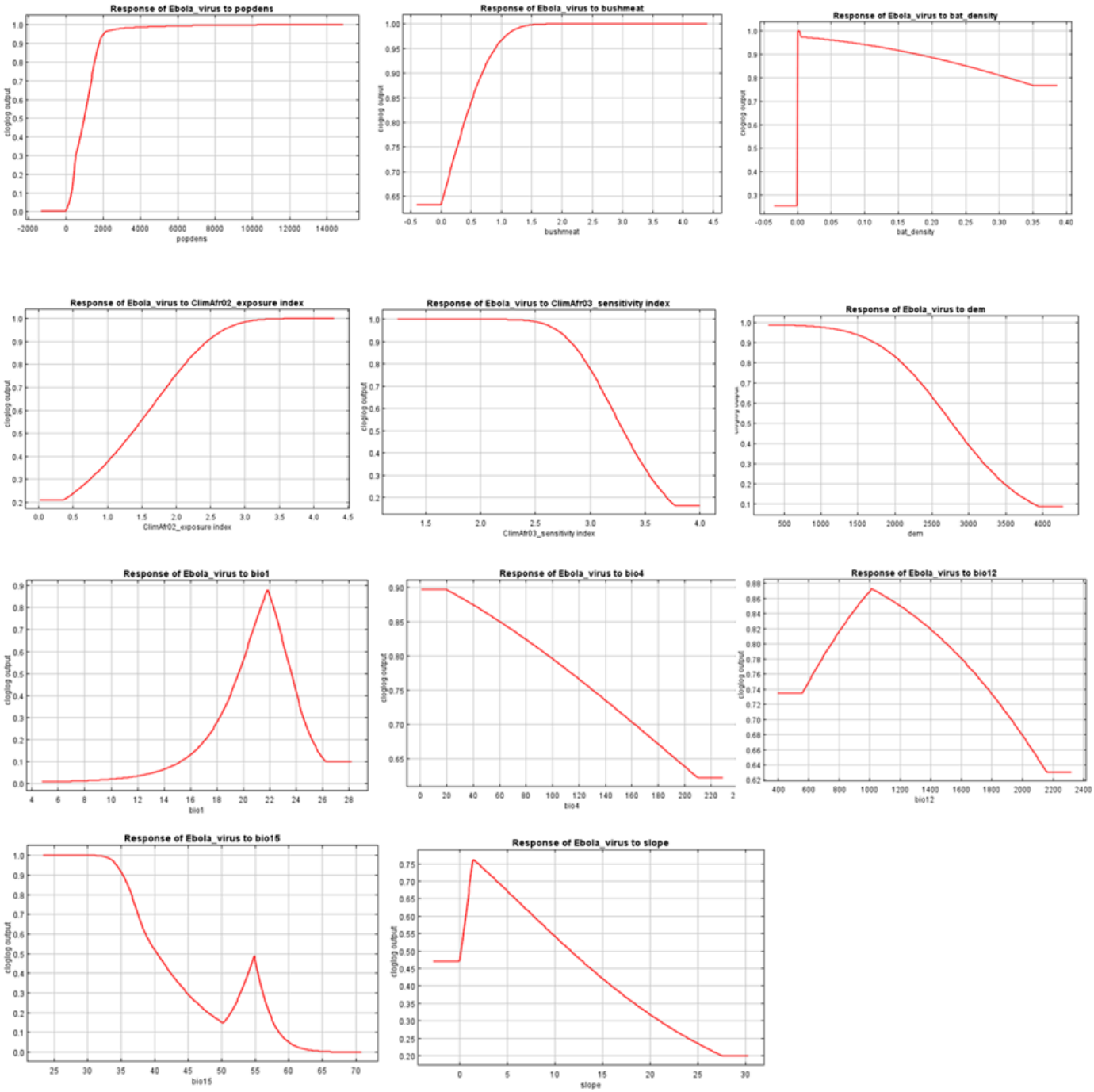

Figure 4

Marginal response curves for the all-species Ebola MaxEnt model. Panels show clog-log output versus covariates.

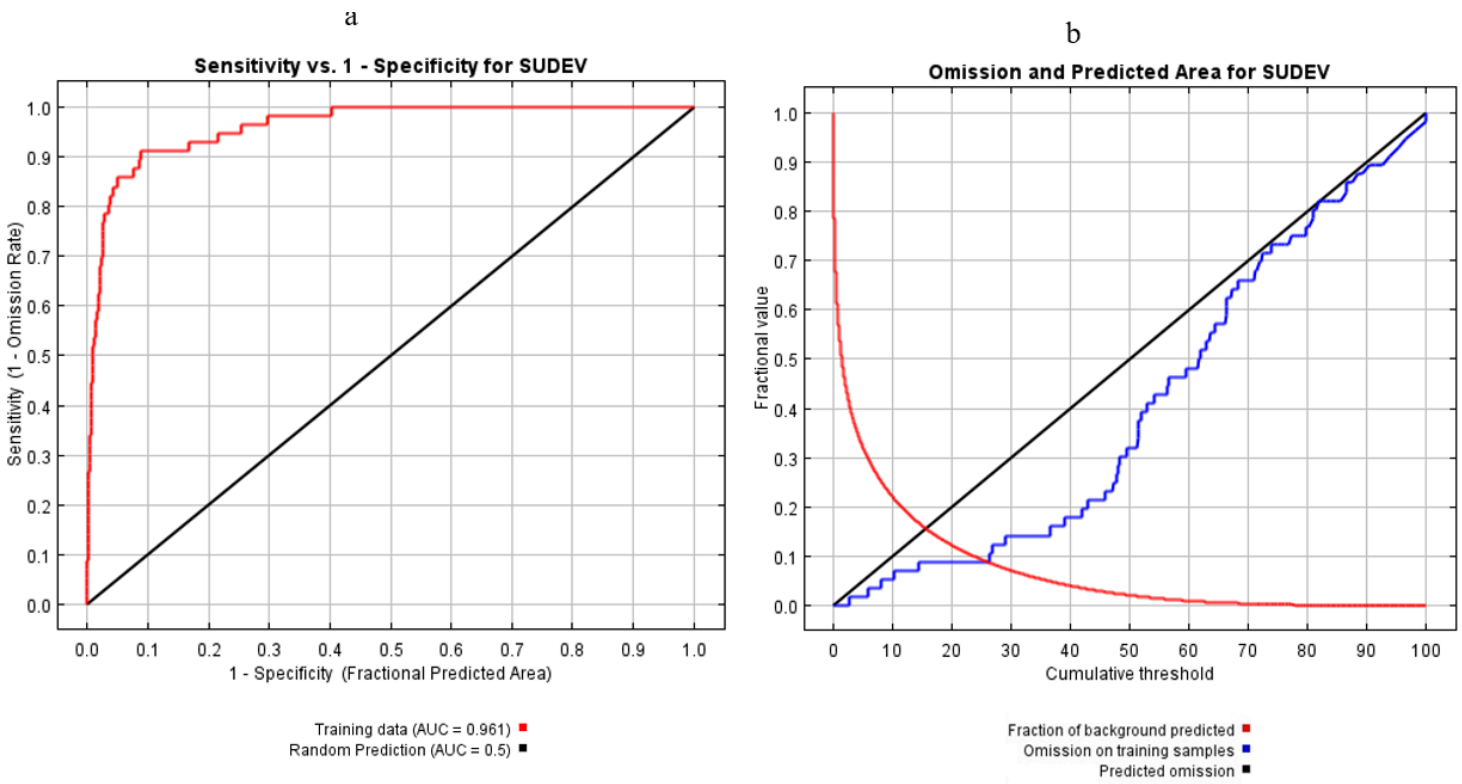

Figure 5

a) Receiver-operator characteristic (ROC) curve for the SUDV-species Maxent model. b) Omission-predicted-area plot justifying the 10 % training-presence clog-log threshold.

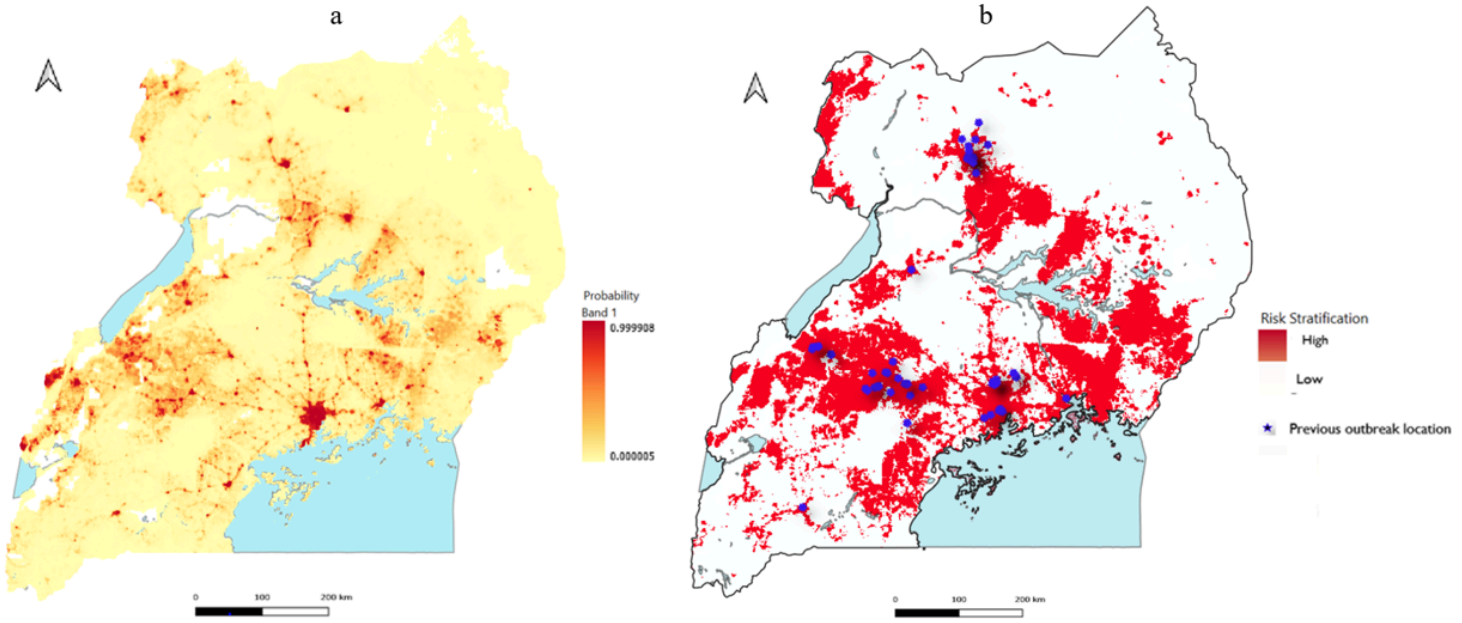

Figure 6

a) Continuous suitability map for Sudan ebolavirus (SUDV) in Uganda. Colour ramp is clog-log probability from 0 (yellow) to 1 (dark red); lakes are shown in pale blue. b) Binary high-risk mask with outbreak

points

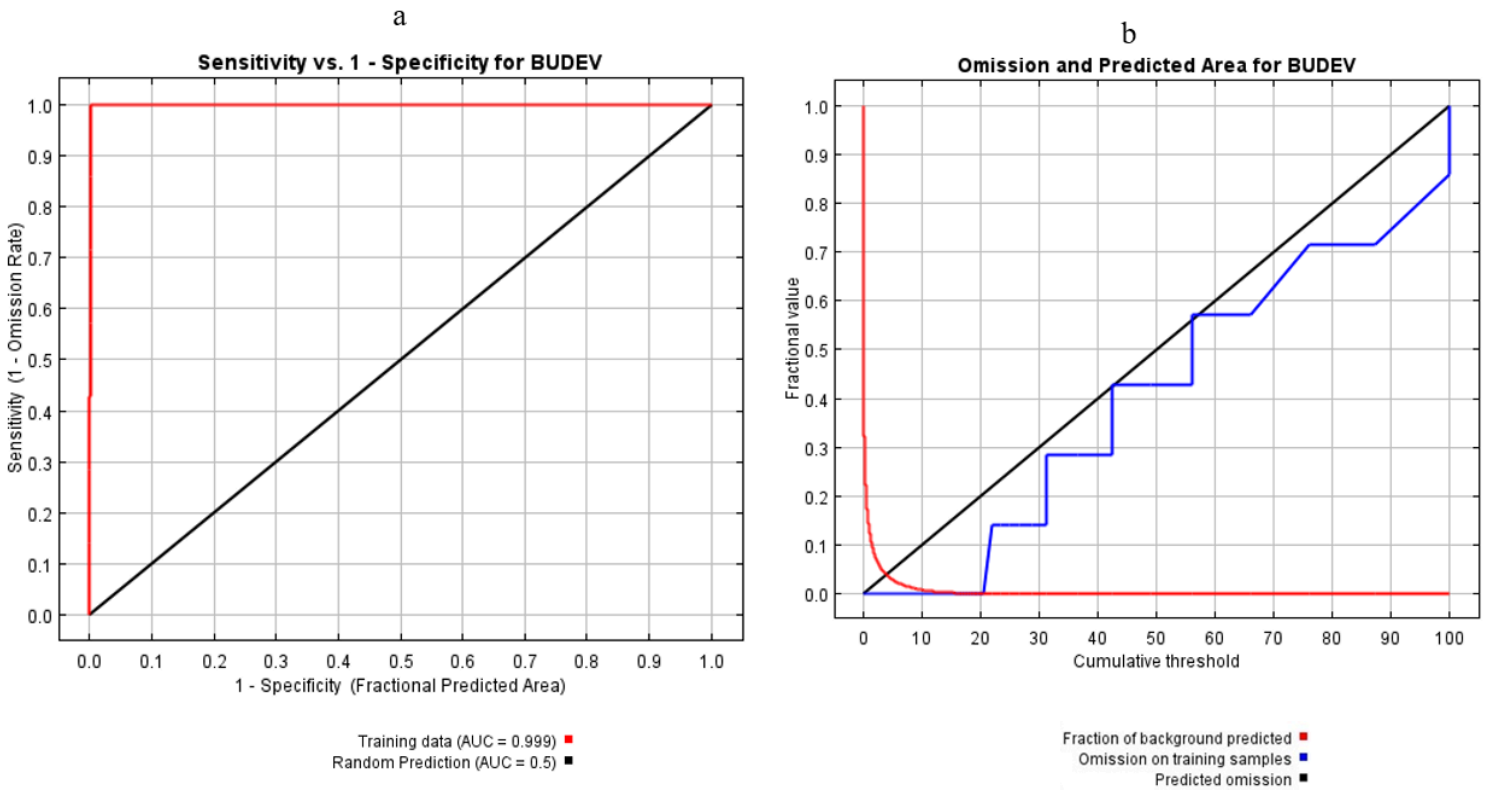

Figure 7

a) Receiver-operator characteristic (ROC) curve for the BDBV-species Maxent model. b) Omission-predicted-area plot justifying the 10 % training-presence clog-log threshold.

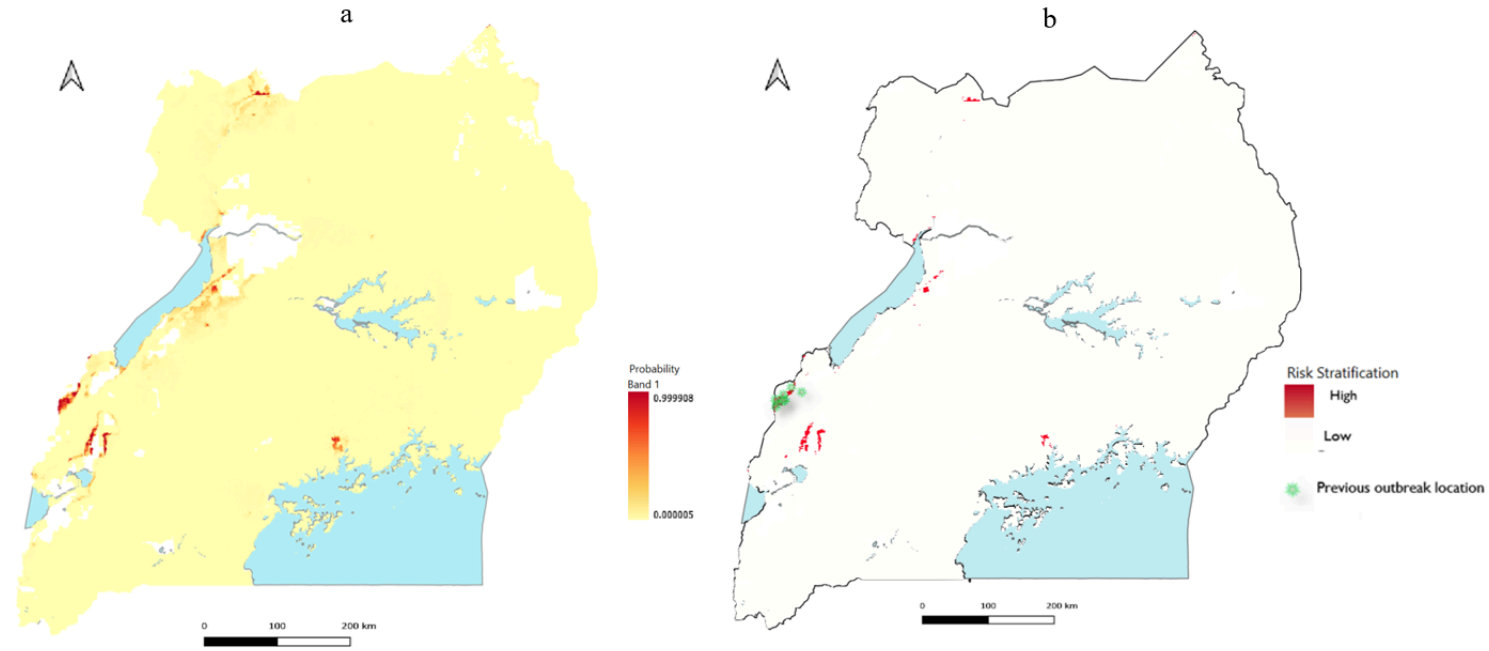

Figure 8

a) Continuous suitability map for Bundibugyo ebolavirus (BDBV) in Uganda. Colours denote clog-log probability; lakes appear in pale blue. b) Binary high-risk mask with outbreak points

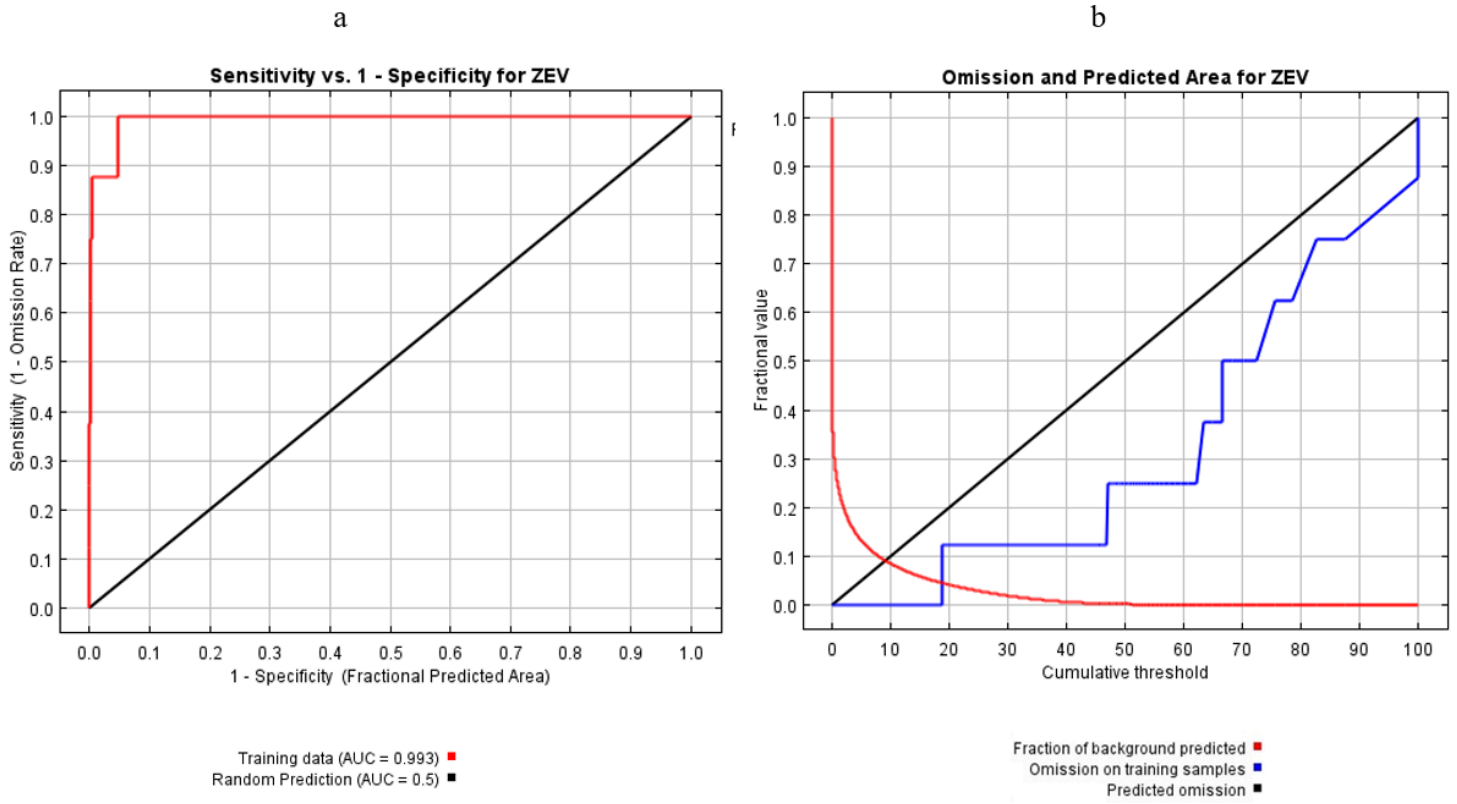

Figure 9

a) Receiver-operator characteristic (ROC) curve for the EBOV-species Maxent model. b) Omission-predicted-area plot justifying the 10 % training-presence clog-log threshold.

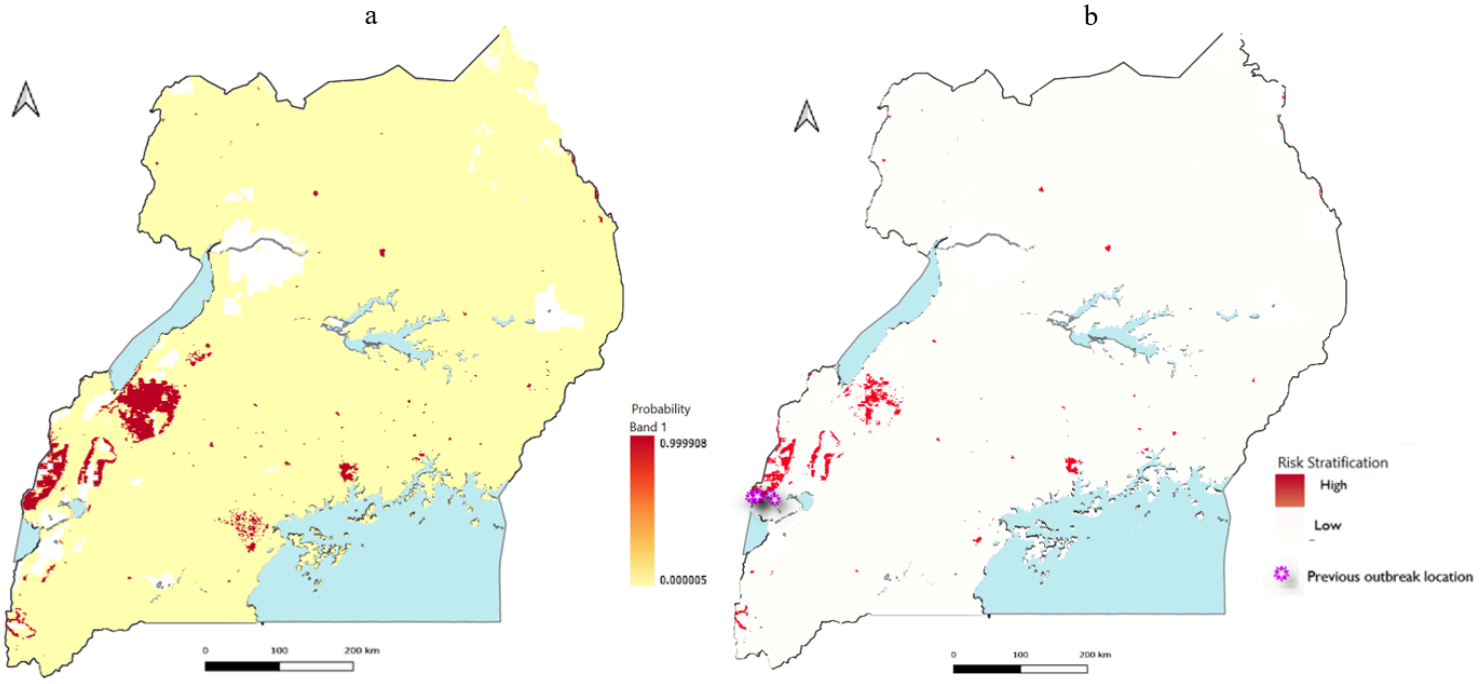

Figure 10

a) Predicted suitability for Zaire ebolavirus in Uganda. Highest probabilities (dark red) form a continuous belt within 40 km of the DRC border. b) Binary high-risk mask with outbreak points

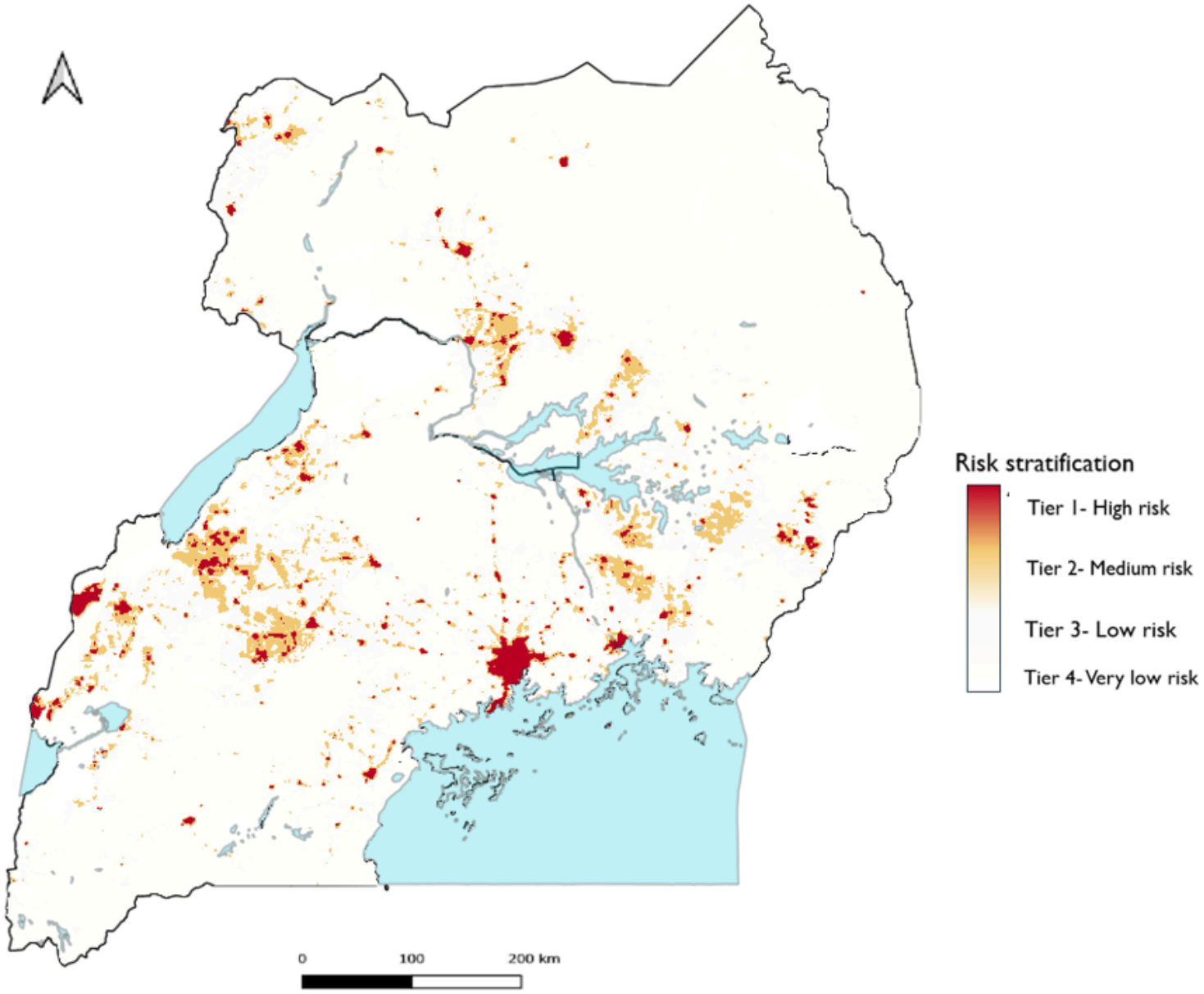

Figure 11

Four-tier Ebola spill-over risk map for Uganda. Continuous MaxEnt probabilities were binarized at the 10 % presence threshold (clog-log = 0.084) and further split at the 50th (≈ 0.28) and 90th (≈ 0.65) percentiles to yield very-low (cream).